LAWRENCE
LIVERMORE
NATIONAL
LABORATORY

UCRL-JC-150052

Quantifying Flaw Characteristics from IR NDE Data

W. O. Miller, N. R. Philips, M. W. Burke, C. L. Robbins

February 14, 2003

Thermosense XXV
Orlando, Florida, April 21-25, 2003

Quantifying flaw characteristics from IR NDE data

Wayne O. Miller[a], Noah R. Philips[b], Michael W. Burke[a], Christopher L. Robbins[a]
[a]Lawrence Livermore National Laboratory, 7000 East Ave., Livermore, CA 94550
[b]Dept. Of Chemistry, Harvey Mudd College, 301 E. 12th St., Claremont, CA 91711

ABSTRACT

Work is presented which allows flaw characteristics to be quantified from the transient IR NDE signature. The goal of this effort was to accurately determine the type, size and depth of flaws revealed with IR NDE, using sonic IR as the example IR NDE technique. Typically an IR NDE experiment will result in a positive qualitative indication of a flaw such as a cold or hot spot in the image, but will not provide quantitative data thereby leaving the practitioner to make educated guesses as to the source of the signal. The technique presented here relies on comparing the transient IR signature to exact heat transfer analytical results for prototypical flaws, using the flaw characteristics as unknown fitting parameters. A nonlinear least squares algorithm is used to evaluate the fitting parameters, which then provide a direct measure of the flaw characteristics that can be mapped to the imaged surface for visual reference. The method uses temperature data for the heat transfer analysis, so radiometric calibration of the IR signal is required. The method provides quantitative data with a single thermal event (e.g. acoustic pulse or flash), as compared to phase-lock techniques that require many events. The work has been tested with numerical data but remains to be validated by experimental data, and that effort is underway. This work was performed under the auspices of the U.S. Department of Energy by Lawrence Livermore National Laboratory under Contract W-7405-Eng-48.

Keywords: Nondestructive Evaluation, Infrared Imaging, Heat Transfer, Least Squares, Signal Processing,

1. INTRODUCTION

Several methods for infrared nondestructive evaluation (IR NDE) are in broad use. Most of these methods rely on transient thermal forcing to illuminate flaws. These include sonic IR that acoustically excites a part to produce heat at a flaw, flash IR that heats the exposed surface of a part with flash lamps, and lock-in methods that can use many types of thermal forcing in a periodic manner. The resulting surface thermal signature from a flaw is governed by heat conduction in the part, and is characterized by a thermal bloom: initial local warming of the surface above the flaw followed by diffuse cooling. This transient thermal signature is the only evidence of a flaw available from IR NDE, and the practitioner must make judgments on the quality of a part by observing and analyzing such signatures, which are indirect measurements of flaws. Such judgments can range from ad-hoc subjective analyses such as just to acknowledge that "something" is producing a signature, to more refined analyses that can sharpen surface detail by image processing, and depth analysis by Fourier methods in the case of lock-in methods. These methods help to define the flaw, but do not truly quantify and describe the flaw in detail. We have developed a method for analyzing the transient thermal signatures that does quantify flaw detail, giving the practitioner better information on which to make judgments of part quality. The method is generally applicable to all transient thermal IR NDE techniques, although the implementation will differ depending on technique.

This work was performed under the auspices of the U.S. Department of Energy by the University of California, Lawrence Livermore National Laboratory under Contract No. W-7405-Eng-48.

A great deal of information on the flaw is contained in the transient thermal signature. The timing of the signature indicates the flaw depth as thermal energy takes time to conduct through the material, and an average flaw depth can be approximated with knowledge of the conduction properties of the material. The size of the flaw can be approximated as roughly equal to the size of the thermal signature, although deeper flaws will produce relatively large signatures as the thermal energy diffuses radially out from the flaw. These approximate results are useful but can be misleading. For example a buried flaw that is neither parallel nor perpendicular to the surface will confound simple attempts to determine both size and depth; size as the flaw area is not fully projected onto the surface, and depth as the flaw exists over a range of depths.

The essence of our technique is to start with a given flaw and analytically predict the resulting thermal signature, rather than working backwards to guess the flaw from the observed signature. The process requires comparing the predicted analytical signature to the observed signature. Once they are in agreement then the flaw has been found that produced the observed signature, including quantified detail on the flaw. Of course flaws vary continuously in size, depth, type and orientation, resulting in an infinite number of possible individual flaws to compare against the observed signature. The task is made tractable by including the variations in size, depth, etc. as free parameters for the analysis, and these parameters are determined when comparing the analytical and observed signatures. Thus the analytical signature is generalized for a prototypical flaw model, which includes the geometry information of the flaw as free parameters. A fitting process whereby the analytical signature is made to match the observed signature determines the free parameters. The scope of the problem is thus reduced from comparing an infinite number of discrete flaws to one of comparing a relatively few number of generalized prototype flaws. Note that all parameters are defined from the analysis for a single thermal event (acoustic pulse, flash), so that lock-in methods for depth determination are not required.

The prototypical flaw models are analytical solutions of the conduction heat transfer process, and depend on the type of thermal forcing used for the IR NDE method (sonic IR, flash IR, etc.). A library of prototypical flaw types is needed to cover flaw variations that cannot be described by the free parameters. Examples of unique prototypical flaw types are surface cracks, buried flaws, and corner cracks. The analytical solutions can be obtained by any appropriate method, and we have initially chosen flaw models that yield to exact analytical results. Other solution options include approximate analytical methods and numerical solutions, although these choices have certain drawbacks for accuracy and computational efficiency. Note that the IR data must be radiometrically calibrated into temperature units in order to compare the analytical and observed thermal signatures.

One goal of this effort is to create an automated capability to analyze IR NDE signatures for quantitative flaw information. We envision a test procedure wherein the IR results from each NDE test are rapidly post processed to extract useful quantitative information. The results of this analysis are then presented to the practitioner as unambiguous data describing the parameters of likely flaws that could produce the input IR signatures. We have achieved significant progress towards this goal and have created all of the fundamental requirements, but have not yet assembled a fully automated capability. In addition, to date we have used only numerically generated thermal data to substitute for radiometric IR signatures, but the experimental effort is moving forward.

2. IR SIGNATURE ANALYSIS

The IR signature analysis involves comparing the observed IR signature to analytically determined best-fit signatures produced by a library of prototypical flaw types, in an effort to determine which flaw type is most likely to produce the

observed signature. The data fitting process required to compare the observed and analytical signatures results directly in quantified information on the prototypical flaw, such as size and depth.

We use the term "prototypical flaw" to mean a flaw of unique type but of undetermined size, depth, etc. For example we will discuss a disk-shaped flaw parallel to the surface but of undetermined radius and depth as one type of prototypical flaw, and a surface crack perpendicular to the surface but of undetermined width and depth as another prototypical flaw. The data fitting process with the observed IR signature determines the unknown parameters, and these parameters are the quantified flaw data.

The analytical signature from a prototypical flaws is the surface temperature around the flaw. The surface temperature is determined by a transient heat transfer analysis as described in the next section. The type of heat transfer analysis depends on the IR NDE method being used. The heat transfer analysis for the prototypical flaws predicts surface temperatures, not IR signal intensity. As a result the observed IR signal must be radiometrically calibrated into temperature units. Only relative temperatures need to be known. The absolute temperature level is not required.

The comparison of observed and analytical signatures requires that the analytical results be numerically fitted to the radiometric IR data. The unknown flaw parameters are also the fitting parameters. We employ a least-squares method to fit the parameters to the data and minimize the fitting error. The analytical expressions for the surface temperatures are nonlinear in the fitting parameters, so we are required to use a nonlinear least-squares fitting routine. There are many such routines available and we have chosen to implement the Levenburg-Marquardt method, which is a standard nonlinear least-squares routine[1].

One issue to consider is how to register the analytical signature to the observed signature, as suggested in Figure 1. In order to fit the data for the complete two-dimensional thermal signature, it would be necessary to include the registration offsets $\Delta\mathbf{x}$ and $\Delta\mathbf{y}$ along with the other fitting parameters, and also to find a solution where these offsets were both zero in order to align the observed data to the analytical data. This is possible but would significantly complicate the fitting process. A related issue is the choice of fitting the complete two-dimensional signature or just selected points within the signature. Again it is possible to fit the complete two-dimensional signature, but at a cost of time and complexity that may not be required.

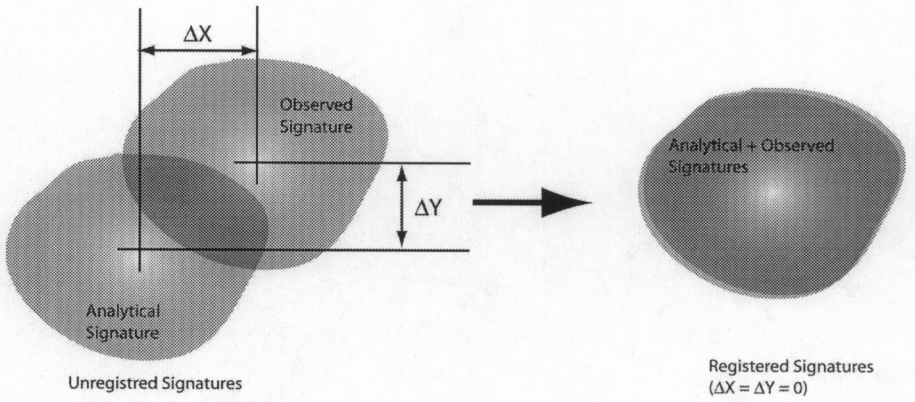

Figure 1. Registration of analytical and observed thermal signatures. Grayscale represents temperature variation.

We have chosen a simplified procedure that requires neither registration nor a complete two-dimensional fitting solution. In this simplified procedure, a single critical point from the analytical signature is fit against all points in the two-dimensional observed signature. The flaw parameters are computed as if each point in the observed signature was properly registered over the single critical point from the analytical solution. As a result, only the single point in the observed signature that corresponds to the critical point will yield the correct solution for the flaw parameters, as only these two points are correctly registered. Note however that only one correct solution point is required to completely solve for all of the flaw parameters, so that if this single registered point can be identified then the solution at that point is all that is required.

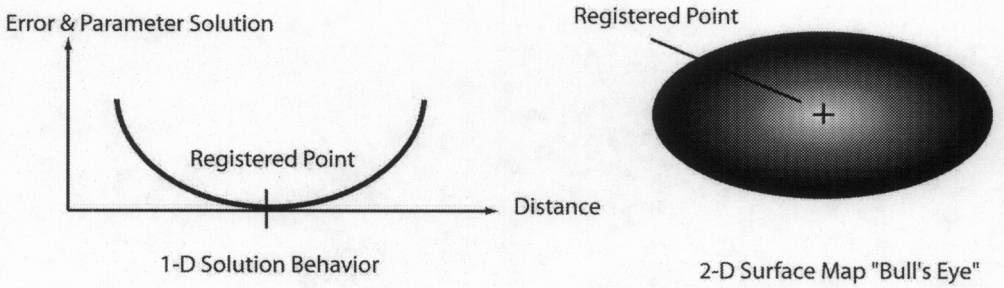

Figure 2. Solution behavior for single point fit showing local extremum at the registered point and bull's eye target for surface maps. Surface map grayscale represents solution parameter magnitude. Surface maps may elongate along flaw dimensions.

The registered point is identified by noting that the solution error will increase with distance from that point. In effect this places the registered point at a local maximum or minimum for each computed flaw parameter, and such points are readily observed as peaks or valleys in the solution (Figure 2). In other words, a surface map of the solution shows the registered point at the center of a bull's eye target[A]. The solution at the center of the target is correct, and becomes increasingly inaccurate with distance from the target center. We have found that this error growth can lead to failure of the least squares solution at some radius from the target point, which further aids to identify the point as the solution domain boundary encircles the target point.

The parameter fitting process and subsequent data analysis have been developed as an interactive MATLAB script. MATLAB is a commercial software product that is suited for numerical and visual analysis of array data, and for rapid software development cycles[2]. We found a significant performance penalty on the least squares routine when MATLAB was running scripts from its native high-level language. In some cases a single signature analysis would require many hours to complete. However it is possible to encode the core numerical procedures in C or FORTRAN subroutines, which are compiled and called from MATLAB scripts. Compiled routines are faster by one or two orders of magnitude in our experience, which indicates that we can achieve a rapid turnaround from camera image to data presentation.

To perform an analysis, the IR image movie is read in and the material thermal properties are entered. The input user interface is shown in Figure 3. The least-squares routine is applied using the single-point method just described to compute the flaw parameters at each pixel in the IR image, based on the transient thermal response at each pixel. The results are presented as surface images of the part when the least-squares analysis is complete. One image is produced

---

[A] The bull's eye target is not in general perfectly circular, but will become elongated to follow the flaw dimensions.

for each of the computed flaw parameters, including a scale of the solution magnitude. The images are visually scanned to locate the registration point bull's eye, and the parameter values at that point are read off. The output also includes statistics on the quality of the least-squares fit.

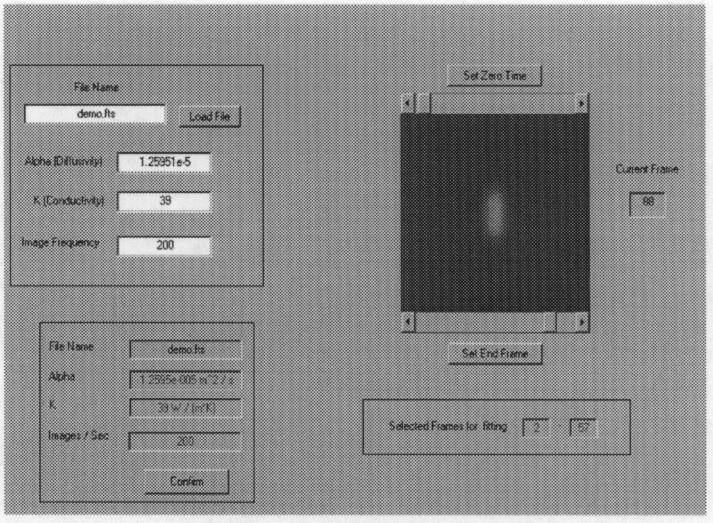

Figure 3. Analysis input interface

3. PROTOTYPICAL FLAW MODELS

The prototypical flaw models define the transient heat transfer behavior for each type of flaw in the flaw library. The observed IR signature is compared to the analytical solution for each flaw type in the library to determine the most likely flaw type that could produce the observed signature. A complete library of prototypical flaw types would include various surface penetrating flaws, buried flaws, flaws at inside and outside corners, etc. We have so far developed two flaw models, a surface penetrating flaw and a buried flaw, as described below. It is conceivable that a single general flaw model could be developed that includes all flaw types as parameter variations, although it appears that the complexity of such a model would likely be prohibitive to its use.

The prototypical flaw models are solutions of the general three-dimensional boundary value problem of heat conduction shown below. Equation (1-a) is the governing differential equation for the temperature $T(\mathbf{r}, t)$, where $\mathbf{r}$ is the position vector and t is time. The thermal conductivity and diffusivity are k and α respectively. The heat generation term is $g(\mathbf{r}, t)$ with typical units of W/m^3. Equation (1-b) is the boundary condition at surface S_i, which is repeated for all surfaces as needed. We have assumed insulated boundaries with no convective heat loss for the two models that follow, for which $h_i = 0$ and $f_i(\mathbf{r}, t) = 0$. Finally equation (1-c) is the initial temperature, and we have assumed a zero initial temperature, $F(\mathbf{r}) = 0$, without loss of generality.

$$\nabla^2 T(\mathbf{r},t) + \frac{1}{k} g(\mathbf{r},t) = \frac{1}{\alpha} \frac{\partial T(\mathbf{r},t)}{\partial t} \quad \text{in region } R,\ t > 0 \tag{1-a}$$

$$k_i \frac{\partial T}{\partial n_i} + h_i T = f_i(\mathbf{r},t) \quad \text{on boundary } S_i,\ t > 0 \tag{1-b}$$

$$T(\mathbf{r},t) = F(\mathbf{r}) \quad \text{for } t = 0, \text{ in region } R \tag{1-c}$$

Exact analytical solutions for the flaw heat transfer behavior are desirable for both speed and accuracy. Exact solutions are written as fairly compact expressions of common mathematical functions that are readily computed. In contrast approximate solutions may require iteration and numerical integration, which are comparatively inefficient and inaccurate operations. Some situations may require approximate solutions, although we have focused on prototypical flaws that yield to exact solutions. In addition we have so far chosen flaw types that result in exact solutions that do not involve infinite series, in order to avoid the necessarily approximate evaluation of such series. Infinite series arise in the solutions when the solution domain is finite, such as for plates of finite thickness. The two flaw types below are for semi-infinite domains. The heat transfer solution for a semi-infinite domain is a reasonable model for thick materials, and for thin materials where the flaw is close to the observed surface so that the boundary effects of other surfaces are not dominant during the short time of interest for IR NDE imaging. However some situations may require solutions that properly account for material thickness, such as a through crack in a thin plate.

Both sonic IR and flash IR NDE techniques rely on the brief input of thermal energy to illuminate the flaw. For sonic IR the heat generation occurs at the flaw site and for flash IR heat generation occurs on the exposed surface. This requires that the heat generation term $g(\mathbf{r}, t)$ be included in the solution, which results in a non-homogeneous differential equation as the heating term is like a forcing function. This class of non-homogeneous problem can be solved by using a Green's function to integrate the differential equation[3]. Green's functions for the heat conduction problem are available for basic geometries such as rectangular, cylindrical and spherical, and for infinite, semi-infinite and finite domains. In the two models that follow we have assumed impulsive heating, so that all of the thermal power is instantaneously delivered to the material at $t = 0$. It is certainly possible to include finite heating time in the solution, and we have shown an example of that for a buried flaw with sonic IR heating in another article[4].

3.1 Surface crack

The prototypical surface crack model for sonic IR is a rectangular crack perpendicular to the surface as shown in Figure 4. The crack penetrates the surface, and has length l along the x-axis and depth d along the z-axis. The solution domain is infinite in the plane ($-\infty < \{x, y\} < \infty$) and semi-infinite in depth ($z > 0$). The crack is impulsively heated at $t = 0$ over the crack area by an amount g_{iA}, which has units of energy per unit area such as J/m^2. This heating is assumed uniform over the crack area.

The unknown parameters for this model are the length l, depth d, and surface heating g_{iA}. These parameters are computed during the least-squares solution. Note that this has the advantage of not requiring knowledge of the sonic IR heating energy, as g_{iA} is computed directly from the thermal response. The same advantage would be found for flash IR modeling as the flash heating energy would also be determined from the solution.

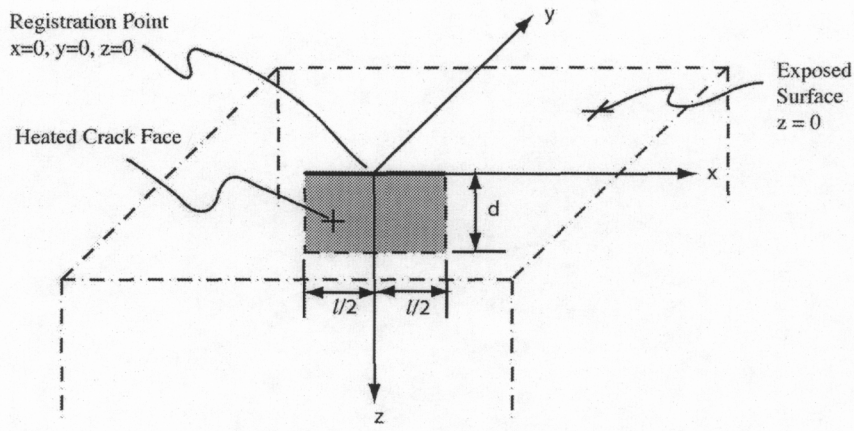

Figure 4. Prototypical surface crack model for sonic IR. Unknown parameters are length l, depth d, and impulsive crack heating g_{iA}.

The two-dimensional surface temperature solution for this model is given in Eq. (2), where *erf*() is the error function. This will yield the full transient two-dimensional thermal signature suggested in Figure 1, with a local hot spot over the crack diminishing with distance from the crack. We use the surface point centered over the crack for the single registration point, which is at the origin {x=0,y=0,z=0}. The solution for this point is given in Eq. (3). This point will have the largest temperature rise of all surface points and is symmetrically located.

$$T(x,y,z,t)=\left(\frac{g_{iA}\sqrt{\alpha}\pi^{3/2}}{2k\sqrt{t}}\right)\left(erf\left(\frac{l/2-x}{2\sqrt{\alpha t}}\right)+erf\left(\frac{l/2+x}{2\sqrt{\alpha t}}\right)\right)erf\left(\frac{d}{2\sqrt{\alpha t}}\right)e^{\frac{-y^2}{4\alpha t}} \quad \text{on surface z = 0} \tag{2}$$

$$T(x,y,z,t)=\left(\frac{g_{iA}\sqrt{\alpha}\pi^{3/2}}{k\sqrt{t}}\right)erf\left(\frac{l/2}{2\sqrt{\alpha t}}\right)erf\left(\frac{d}{2\sqrt{\alpha t}}\right) \quad \text{at point } \{x = 0,\ y = 0,\ z = 0\} \tag{3}$$

3.2 Buried flaw

The prototypical buried flaw model for sonic IR is a disk-shaped flaw parallel to the surface as shown in Figure 5. This type of flaw might represent a crack, delamination, or other subsurface defect. The flaw has radius R and is buried at depth a along the z-axis. The solution coordinate system is cylindrical, and the domain is infinite in radius ($0 < r < \infty$) and semi-infinite in depth ($z > 0$). The flaw is impulsively heated at $t = 0$ over the flaw area by an amount g_{iA} and this heating is assumed uniform over the flaw area. The unknown parameters for this model are the radius R, depth a, and surface heating g_{iA}. These parameters are computed during the least-squares solution.

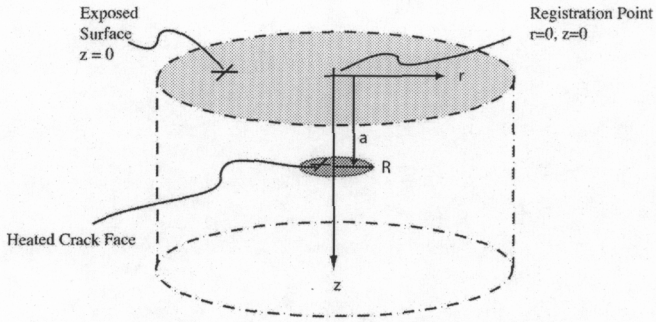

Figure 5. Prototypical buried flaw model for sonic IR. Unknown parameters are radius R, depth a, and impulsive flaw heating g_{iA}.

The two-dimensional surface temperature solution for this model is given in Eq. (4), where $I_0()$ is the zero-order modified Bessel function of the first kind. No compact solution was found for the integral appearing in Eq. (4), which would thus require numerical integration to evaluate in the given form. A compact solution was obtained for the single registration point at {r=0, z=0}, which is centered above the disk flaw on the surface. This solution is given in Eq. (5). This point will have the largest temperature rise of all surface points and is symmetrically located.

$$T(r,z,t) = \frac{\alpha g_{iA}}{2k\sqrt{\pi}(\alpha t)^{3/2}} e^{\frac{-a^2}{4\alpha t}} e^{\frac{-r^2}{4\alpha t}} \int_{\rho=0}^{R} e^{\frac{-\rho^2}{4\alpha t}} I_o\left(\frac{r\rho}{2\alpha t}\right) \rho d\rho \quad \text{on surface z = 0} \tag{4}$$

$$T(r,z,t) = \frac{\alpha g_{iA}}{k\sqrt{\pi\alpha t}} e^{\frac{-a^2}{4\alpha t}} \left(1 - e^{\frac{-R^2}{4\alpha t}}\right) \quad \text{at point } \{\text{r=0, z=0}\} \tag{5}$$

4. NUMERICAL EXAMPLE

The example case offered is based on fitting the analytical solution for the knife-edge surface crack to a numerically evaluated thermal model of the same crack geometry. We did not have experimental radiometric data available for this initial attempt. Nonetheless the numerical example is predictive of results with experimental IR data that is accurately calibrated to temperature.

The numerical model was for a crack 2mm deep (d) and 2mm long (l) with 1000 J/m^2 of impulsive heating (g_{iA}). The material properties were for aluminum oxide. This resulted in an impulsive temperature rise of approximately 7 °C along the surface crack edge. Figure 6 shows a thermal map of the surface for early and late times after the impulsive heating. At early times the thermal energy is concentrated around the crack while at late times the energy diffuses by conduction.

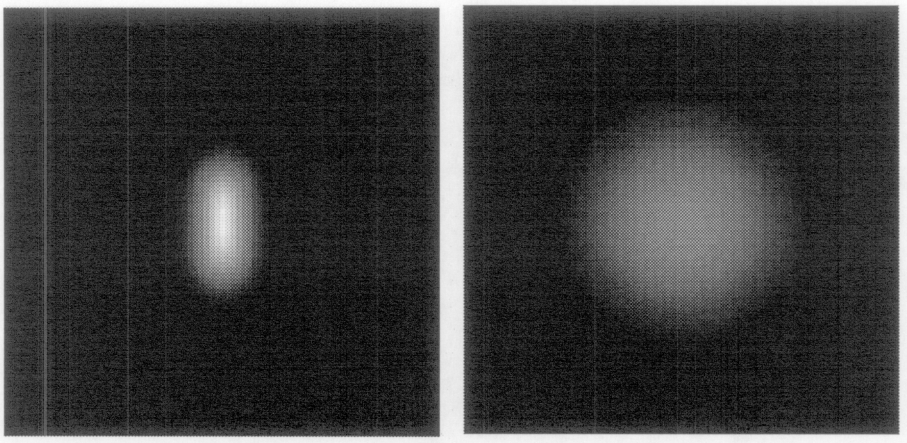

Figure 6. Thermal response of knife-edge crack at early and late times. Lighter color indicates warmer temperature.

The thermal history from the numerical model was input into the analysis software just as if it was a calibrated IR signature, and the least-squares fitting process was performed on the data. The fitting parameters l, d, and g_{iA} were accurately determined at the single registration point. An example of the resulting parameter maps is shown in Figure 7, which shows the predicted crack depth over the surface of the image. This image was originally in color and is best shown in color as the rendered gray scale image shown here does not clearly correspond with the scale bar showing the crack depth magnitude. However as indicated on the figure, the predicted depth is accurate at the registration point at the crack center. Note that the predicted solution appears as an elongated bull's eye centered over the registration point and aligned with the crack dimension, and also that the solution failed to converge for depths larger than 5mm, producing a border around the bull's eye. It is also seen that the error grows slowly with distance from the registration point, allowing for some imprecision in locating the registration point.

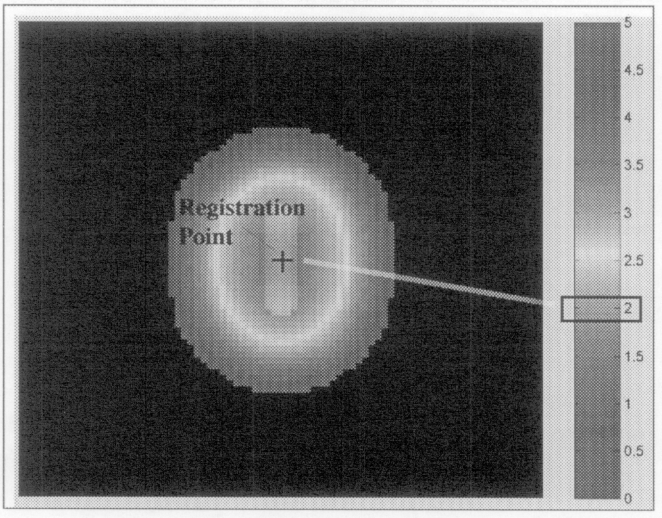

Figure 7. Solution for crack depth for a knife-edge surface crack. Scale values are predicted crack depth in mm. The correct 2-mm depth is accurately predicted at the registration point. Solution shows elongated bull's eye target shape centered on

registration point, and solution failure beyond a certain radius. Gray scale was rendered from original color resulting in loss of visual information.

5. CONCLUSIONS

A technique has been demonstrated that can extract quantified flaw information from transient IR NDE data. The NDE practitioner can use this technique to accurately define the flaw that produced a given IR signature. The method is applicable to any transient thermal IR NDE method, such as sonic IR and flash IR.

When fully developed the technique is intended to compare the observed IR signature to a library of prototypical flaw types to determine the flaw type that produced the observed signature, and to do so in a rapid automated fashion. At present only individual flaw types are addressed as the library capability is being developed. The analysis software has been implemented as an interactive MATLAB script. The practitioner inputs the observed IR signature movie and the material thermal properties in order to start the solution.

The flaw parameters (size, depth, etc.) are determined by fitting free parameters in analytically derived thermal models to the observed IR signature. A nonlinear least-squares routine is used for the fitting process. The results of the fitting process are solution maps for each parameter that can be superimposed on the original IR image. Comparison of the observed and analytical signatures requires that the observed IR data be radiometrically calibrated into temperature units.

We have chosen to implement a single-point registration method wherein only one point of the solution map is guaranteed to be accurate, however only one point is needed for a complete parameter solution. This single registration point corresponds to perfect alignment of the observed and analytical thermal signatures. The benefits of this method are that there is no need to align the two-dimensional observed and analytical thermal signatures, either visually or numerically, and that the analytical solution need only be known at a single point on the surface. The registration point is readily identified in the parameter solution maps as the center of a bull's eye target.

REFERENCES

1. Press, W. H., Teukolsky, S. A., Vetterling, W. T. and Flannery, B. P., *Numerical Recipes in FORTRAN, The Art of Scientific Computing*, 2nd Ed., Cambridge University Press, 1992, pp. 678-683.

2. *Using MATLAB Version 6*, The MathWorks, Inc., Natick, MA, 2000.

3. Ozisik, M. N., *Heat Conduction*, John Wiley and Sons, New York, 1980.

4. Miller, W. O., Darnel, I. M., Burke, M. W., Robbins, C. L., "Defining the envelope for sonic IR: detection limits and damage limits," *Thermosense XXV*, Maldague, X. P. and Rozlosnik, A. E., eds., SPIE, Orlando, FL., April 22-24, 2003.